Title
Powering Triton's recent geological activity by obliquity tides: Implications for Pluto geology

Journal
Icarus, 246

ISSN
00191035

Authors
Nimmo, F.
Spencer, J.R.

Publication Date
2015

DOI
10.1016/j.icarus.2014.01.044

Peer reviewed

Powering Triton's recent geological activity by obliquity tides: Implications for Pluto geology

F.Nimmo [a] J. R. Spencer [b]

[a] *Dept. Earth and Planetary Sciences, University of California, Santa Cruz, 1156 High St., Santa Cruz, CA 95064, USA*

[b] *Southwest Research Institute, 1050 Walnut St. Suite 300, Boulder CO 80302, USA*

Number of pages: 27
Number of tables: 2
Number of figures: 3

Preprint submitted to Icarus *29 January 2014*

Proposed Running Head:
Triton obliquity tidal heating

Please send Editorial Correspondence to:

Francis Nimmo
Dept. of Earth and Planetary Sciences, University of California, Santa Cruz
1156 High St.
Santa Cruz, CA, 95064, USA.

Email: fnimmo@es.ucsc.edu
Phone: (831) 459-1783

ABSTRACT

We investigate the origins of Triton's deformed and young surface. Assuming Triton was captured early in solar system history, the bulk of the energy released during capture will have been lost, and cannot be responsible for its present-day activity. Radiogenic heating is sufficient to maintain a long-lived ocean beneath a conductive ice shell, but insufficient to cause convective deformation and yielding at the surface. However, Triton's high inclination likely causes a significant ($\approx 0.7°$) obliquity, resulting in large heat fluxes due to tidal dissipation in any subsurface ocean. For a 300 km thick ice shell, the estimated ocean heat production rate ($\approx$0.3 TW) is capable of producing surface yielding and mobile-lid convection. Requiring convection places an upper bound on the ice shell viscosity, while the requirement for yielding imposes a lower bound. Both bounds can be satisfied with an ocean temperature $\approx$240 K for our nominal temperature-viscosity relationship, suggesting the presence of an antifreeze such as NH_3. In our view, Triton's geological activity is driven by obliquity tides, which arise because of its inclination. In contrast, Pluto is unlikely to be experiencing significant tidal heating. While Pluto may have experienced ancient tectonic deformation, we do not anticipate seeing the kind of young, deformed surfaces seen at Triton.

Keywords: Satellites, dynamics ; Tides, solid body ; Pluto ; Triton

1 Introduction

In terms of their bulk properties, Triton and Pluto are remarkably similar (see Table 1). Both are presumed to have formed as Kuiper Belt objects, although retrograde Triton was captured into Neptune orbit at some point in its history (McKinnon and Kirk, 2007). Triton has a young (<100 Myr) surface (Schenk and Zahnle, 2007), deformed by a variety of tectonic and possibly cryovolcanic (Croft et al., 1995) features, and exhibits geysers that are probably powered by solar heating (Kirk et al., 1990). It is therefore of interest to consider the question: to what extent will Pluto resemble Triton?

In this MS we lean heavily on Triton's youthful appearance in assessing its likely interior state. With Pluto, firm predictions are elusive. However, we argue that *New Horizons* observations will not only clarify Pluto's interior state, but will also determine whether our favoured hypothesis for Triton's activity is correct.

The logic of the MS is as follows. We first demonstrate that the heat released during Triton's orbital evolution following capture only marginally affects its present-day behaviour (Section 3.1). Based on its young apparent age, we assume that Triton's icy surface is being deformed, at least in part, by convection (Stern and McKinnon, 2000, c.f.), as similarly young surfaces on Europa and Enceladus are thought to do. We then argue that surface deformation and yielding require heat fluxes much greater than Triton's radiogenic elements can supply (Section 3.2). However, the addition of tidal heating is sufficient to permit yielding to occur, and also makes a long-lived ocean possible. As argued by Jankowski et al. (1989), Triton's odd orbital configuration makes heating by obliquity tides unusually effective. In contrast to these authors, however, we focus on dissipation within a subsurface ocean (Section 3.3). A Triton consisting of a thick convecting ice shell overlying a long-lived, cold (and currently dissipative) ocean is energetically plausible and consistent with the meagre observational constraints.

How does this picture relate to Pluto? The main difference is that tidal heating is unlikely to operate at Pluto and, as a result, surface yielding should not be occurring currently. If our scenario regarding Triton's extra energy source is correct, Pluto should show no signs of recent geological activity. Conversely, if Pluto's surface does turn out to be as young as Triton's, this suggests that processes other than tidal heating are likely responsible for the activity of both moons. One possible explanation in this case would be the presence of highly volatile species enabling geological activity powered by radiogenic heat alone.

Because of the relative paucity of observational constraints compared to e.g. the Saturnian or Jovian satellites, we have favoured order-of-magnitude arguments over detailed models wherever possible. Uncertainties are generally so large that exploring parameter space with complex models is impractical, and unlikely to yield additional insight beyond the simple calculations presented here. We do, however, identify some questions which may be worth exploring in more detail.

1.1 Observations

An important clue to Triton's present-day state is the fact that its surface is so lightly cratered, suggesting a surface age less than at most 100 Myr old (Schenk and Zahnle, 2007). There are only four other known outer solar system bodies with comparable surface ages. Titan and Io are unsuitable analogues, because the resurfacing is due in large part to erosion/sedimentation, and prodigious silicate volcanism, respectively. Europa's heavily deformed surface is about 50 Myr old on average (Zahnle et al., 2003), while the south polar region of Enceladus is probably even younger

(Porco et al., 2006). In both cases, resurfacing is plausibly due to deformation driven by convection involving motion of the entire near-surface lid (Showman and Han, 2005; Barr, 2008; O'Neill and Nimmo, 2010). In both cases the ultimate energy source driving this motion is tidal heating. Given the abundance of plausibly tectonic features on Triton's surface (Croft et al., 1995), we shall assume below that convection-related yielding and deformation is taking place. We note, however, the possibility that mechanisms other than ice shell convection, such as cryovolcanism (Croft et al., 1995) or diapirism driven by local density variations (Schenk and Jackson, 1993) may also contribute to Triton's resurfacing.

While Triton is also active up to the present time in the sense that it has active geysers, we do not view this as a particularly useful constraint. Although the geysers at Enceladus are probably related to its internally active state, Triton's geyser activity is plausibly driven by solar heating (Kirk et al., 1990) rather than endogenic geological activity.

1.2 Orbital history

Triton's retograde orbit indicates that it was captured. Three capture mechanisms have been proposed: aerodynamic drag (McKinnon and Leith, 1995); collision with another satellite (Goldreich et al., 1989); and exchange capture (Agnor and Hamilton, 2006). Of these, the last - in which a binary object encounters Neptune and one member of the binary (Triton) is captured - is by far the most probable. The timing of the capture event is somewhat unclear. Aerodynamic drag can only have operated during Neptune's formation, and the probability of a collision, always low, becomes much lower once the main stage of accretion ended. Exchange capture could in theory occur at any time, but modelling by Vokrouhlicky et al. (2008) suggests that it probably happened within the first 5-10 Myr of solar system history.

The conventional picture of Triton's post-capture orbital evolution may be divided into two phases (Chyba et al., 1989; Ross and Schubert, 1990). In the first phase, its initially highly eccentric orbit was circularized by tidally-driven dissipation. Because of the strong positive feedback between dissipation and temperature, the majority of the circularization probably took place rapidly ($<$100 My). The duration of the entire circularization process depends on poorly-known rheological parameters, but was almost certainly $<$1000 Myr. An alternative, more rapid ($\sim$0.1 My) mode of circularization is via interaction with a disk resulting from collisions between other pre-existing satellites (Cuk and Gladman, 2005). In either case, the end state was a body on an inclined, but essentially circular orbit.

The second phase involves more gradual evolution to the present-day situation. Tidal dissipation in a satellite damps both eccentricity and inclination, while dissipation in the primary can have the opposite effect (Murray and Dermott, 1999). For the Neptune-Triton system, it is not obvious whether dissipation in the primary or the satellite dominates (Chyba et al., 1989). However, irrespective of this issue, the inclination will damp more slowly than the eccentricity (as is evident from the current circularity of Triton's orbit). We discuss this issue in more detail in Section 3.3 and equation (9) below, and demonstrate that the inclination is not expected to have damped over the age of the solar system. The reason this issue is important is that it is Triton's non-zero inclination which we hypothesize is the ultimate cause of present-day tidal heating (Section 3.3).

2 Structure and parameter choices

For a body consisting of two layers of uniform density, the bulk density ρ_b is given by

$$\rho_b = \rho_i \left(1 + \frac{(\rho_s - \rho_i)}{\rho_i}\left[\frac{R_s}{R}\right]^3\right) \tag{1}$$

where the density of the outer and inner layers are ρ_i and ρ_s, respectively, and the radial position of the interface is R_s. For Triton and Pluto, we assume the outer layer is Ice I (ρ_i=950 kg m^{-3}) and the inner layer is anhydrous silicates plus iron with a density similar to Io's (ρ_s=3500 kg m^{-3}). The resulting radius of the rock-iron core R_s and the maximum thickness of the ice shell d_{max} are given in Table 1. Triton's maximum ice shell thickness is 327 km; a lower density inner layer results in a thinner shell (e.g. 284 km for ρ_s=3200 kg m^{-3}). The actual shell thickness may also be smaller if a subsurface ocean is present.

This simple analysis ignores many details: the role of higher pressure ice phases, the possibility of a hydrated core, porosity in the near-surface of the ice shell, and so on. However, at the order-of-magnitude level that we are discussing, none of these details are likely to matter. One important exception is that Pluto (but not Triton) might not be fully differentiated. We discuss this issue briefly in Section 5.

Whether or not an ocean is present for either Triton or Pluto is unclear (Hussmann et al., 2006; Desch et al., 2009; Gaeman et al., 2012, e.g.). As discussed in Robuchon and Nimmo (2011), a present-day ocean on Pluto is likely if the ice shell is not convecting; conversely, a convecting ice shell prevents an ocean from developing. Whether a similar logic applies to Triton depends on the heat sources available to prevent an ocean from freezing (see Section 3 below). However, in the case of Pluto our principal conclusions do not depend on whether or not an ocean is present.

For ice, we assume a constant thermal conductivity of 3 W m^{-1} K^{-1}. The temperature-dependent conductivity of ice (Klinger, 1980) would result in a higher mean value; on the other hand, the presence of clathrates and/or porous material would lower the conductivity. The uncertainties involved do not significantly affect our conclusions. The viscosity of ice is dependent on temperature, grain size, melt fraction and stress (Goldsby and Kohlstedt, 2001). Where necessary we assume a simple Newtonian rheology with a reference viscosity near the melting point of about 10^{14} Pa s, appropriate for ice with grain size of order 1 mm under the low stresses characteristic of convection. Such grain sizes are appropriate for situations in which pinning by secondary phases prevents grain growth from occurring (Barr and McKinnon, 2007).

Although we do not include them here, the presence of clathrates could affect our results, since they have significantly lower thermal conductivities and higher viscosities than pure water ice (Durham et al., 2010). Both characteristics would tend to allow subsurface oceans to persist for longer. Similarly, we do not include the effects of ices other than water ice. The effect of antifreezes such as NH_3 is also to make a present-day ocean more likely (Hussmann et al., 2006, e.g.).

In the absence of any observational constraints, we adopt a chondritic heating rate using the same parameters used by Robuchon and Nimmo (2011), which yields a present-day radiogenic heat flux of 2.4 mW m^{-2} (or 3.4×10^{-12} W kg^{-1}). This value is a little smaller than the range of $3.3 - 6.6$ mW m^{-2} used by Brown et al. (1991), but almost twice the present-day value of 1.3 mW m^{-2} adopted by Gaeman et al. (2012). Part of the reason for the discrepancy with the latter study is that these authors assumed a differentiated inner layer containing roughly equal iron and silicate mass fractions, and then calculated heat production in the silicate layer alone. This results in an underestimate, because the chondritic heating rates they used are based on undifferentiated materials (i.e. silicates plus iron).

3 Heat Sources

3.1 Primordial Heating

Immediately after capture, Triton's orbit was highly elliptical, leading to large tides. These tides in turn caused heating, reducing Triton's effective rigidity and thus further increasing the amplitude of tidal deformation and heating. This positive feedback probably led to a brief, intense period of heating, up to ∼1 Gyr after capture, after which Triton's orbit was essentially circular (Ross and Schubert, 1990).

The total energy released, expressed as a mean temperature change, is given by (McKinnon and Kirk, 2007, e.g.)

$$\Delta T \approx \frac{G m_p}{2 a C_p} \approx 9600 \text{ K} \tag{2}$$

where m_p is the mass of the tide-raising body (Neptune), a is the semi-major axis and C_p is the mean specific heat capacity ($\approx 10^3$ J kg^{-1} K^{-1}). Evidently circularization was sufficient to cause widespread melting and complete differentiation.

However, Triton's small size means that this initial heat is not readily stored. The diffusion timescale in a sphere of radius R is $R^2/\pi^2\kappa$, where κ is the thermal diffusivity (Carslaw and Jaeger, 1986). For a sphere 1000 km in radius with $\kappa = 10^{-6}$ m^2 s^{-1}, this timescale is 3.2 Gyr, smaller than the age of the solar system. Thus, even in the most conservative case (i.e. neglecting convection and melt transport), primordial heat likely plays only a minor role in the present-day energy budget of Triton.

Figure 1 shows a slightly more sophisticated set of calculations which reinforce this conclusion. Here we are modelling a Triton consisting of a conductive rock-iron core heated by radiogenic decay and an outer H_2O region. This region consists of a conductive ice shell and potentially an ocean. The ocean will melt or freeze depending on the balance between heat transported from the top of the rock-iron layer (here referred to as the ice-core interface or ICI) and heat lost from the shell to space. Further details on the numerical technique employed are presented in the Appendix.

Fig 1a shows a case in which Triton is started from a cold temperature (150 K everywhere). The heat flux from the ICI increases as the rock-iron core heats up due to radioactive decay, and then wanes as the radiogenic elements are exhausted. The ice shell heats up, because heat transfer out of the shell is smaller than the heat being added from the ICI. Once the ice shell exceeds 270 K, it begins to melt. The ice shell reaches a minimum thickness at about 2 Gyr, and then proceeds to slowly refreeze thereafter, with a present-day thickness of 160 km and surface heat flux of 4.0 mW m^{-2}. The present-day surface heat flux and ICI heat flux are almost in balance, which is what one would expect because of the short heat transfer timescale across the ocean and ice shell. Both these heat fluxes exceed the present-day rate of radiogenic heat production (equivalent to 2.4 mW m^{-2} at the surface) because of the time it takes for this heat to diffuse outwards through the rock-iron core. This scenario is very similar to that shown in Figs 2e-f of Robuchon and Nimmo (2011). However, we differ from Gaeman et al. (2012) in that our models are able to maintain an ocean to the present day without requiring tidal heating. The reason is that Gaeman et al. (2012) assumed a silicate core volume of 1.79×10^{17} m^3, which is roughly an order of magnitude too small. As a result, the contribution of radiogenic heating to maintaining an ocean is significantly underestimated (Hier-Majumder, pers.comm.).

Fig 1b shows the same situation, but now with a hot start (1000 K for the core and 250 K for the ice shell). Shell melting occurs almost immediately, and the ICI heat flux shows a monotonic decline because of the initial high temperature. However, the present-day situation is very similar to that shown in Fig 1a - the present-day surface heat flux is 4.9 mW m^{-2} and the shell thickness 130 km. Thus, as expected the initial conditions have only a rather limited effect on the present-day state of the ice shell.

Of course, this simple scenario neglects the possibility of heat transport by convection or advection (of melt). This is important for e.g. the thickness of the shell, and whether or not an ocean exists at the present day (see below). However, because more rapid heat transfer further reduces the influence of primordial heat on Triton's present-day thermal state, including such processes will only strengthen our conclusion that the initial conditions do not affect the present-day energy budget.

Thus, to first order Triton's initial heating should not affect its present-day behavior. Of course, there may be important details; for instance, early volatile loss driven by tidal heating could have important consequences for subsequent behavior. Nonetheless, unless Triton's capture happened late in solar system history - which is highly improbable - its young, deformed surface must be due to processes other than the initial capture event, and whether or not it possesses an ocean now is not sensitive to the initial conditions.

3.2 Convection, conduction and yielding

Fig 1 makes it clear that a present-day ocean on Triton can be sustained by radiogenic heating - assuming that the ice shell is conductive. Contrariwise, based on numerical modeling of Pluto, a convecting shell can be sufficiently efficient at removing heat that an ocean never develops (Robuchon and Nimmo, 2011). Unfortunately, it is hard to decide from a purely theoretical standpoint whether a conductive or convective shell is more likely. Fortunately, what we really care about is whether the surface is deforming or not - and we will argue below that this question can be addressed using a relatively simple criterion.

The viscosity of ice $\eta(T)$ is strongly temperature-dependent (Goldsby and Kohlstedt, 2001, e.g.):

$$\eta(T) = \eta_0 \exp\left[\frac{E_a}{R_g}\left(\frac{1}{T_0} - \frac{1}{T}\right)\right] \tag{3}$$

where η_0 is the reference viscosity at the reference temperature T_0 (=273 K), E_a is the activation energy and R_g is the gas constant. A typical ice reference viscosity is 10^{14} Pa s, but this depends on grain size and impurities (as noted above).

Convection ceases if the Rayleigh number Ra declines below some critical value Ra_{cr}, where Ra is given by

$$Ra = \frac{\rho_i g \alpha (T_b - T_s) d^3}{\kappa \eta_b} \tag{4}$$

with ρ_i the ice density, g the acceleration due to gravity, T_b and T_s the temperatures at the top and bottom of the shell, d the ice shell thickness, α the thermal expansivity, κ the thermal diffusivity and η_b the viscosity at the base of the ice shell, temperature T_b. A measure of the sensitivity of the ice viscosity to a change in temperature is given by $\gamma = E_a/R_g T_b^2$ (Solomatov, 1995), where for ice $\gamma \approx 0.1\ K^{-1}$.

For Newtonian materials the critical Rayleigh number Ra_{cr} is independent of the amplitude of temperature perturbations and is given by

$$Ra_{cr} = 155(\gamma[T_b - T_s])^4 \quad (5)$$

where the prefactor depends on the aspect ratio $[1-(d/R)]$ and is given here for a Triton-like aspect ratio of 0.72 (Robuchon and Nimmo, 2011). For T_b=270 K, $Ra_{cr} \approx 4 \times 10^7$.

Whether or not convection causes surface yielding and deformation depends on how large the convective stresses σ_c are compared to the yield stress of the material σ_y. The convective stresses in the mobile lid regime are given by (Moresi and Solomatov, 1998; Van Heck and Tackley, 2011):

$$\sigma_c \sim \frac{\eta_i \kappa}{\delta_0^2} \sim \frac{\eta_i \kappa}{k^2(T_b - T_s)^2} F_c^2 \quad (6)$$

where η_i is the viscosity of the convecting interior, δ_0 is the thickness of the convecting boundary layer in the mobile-lid regime, F_c is the convective heat flux and the second equality is derived by taking $F_c \approx k(T_b - T_s)/\delta_0$, with k the thermal conductivity. Doubling the heat flux increases the convective stress by a factor of four; thus, more vigorous convection is more likely to cause yielding. The importance of equation (6) is that, for a given viscosity, it can be used to determine a critical convective heat flux below which surface yielding does not take place. Note that there is an implicit dependence on Ra, because the convective heat flux and δ_0 both depend on Ra.

For two different satellites, assuming that $(T_b - T_s)$, k and κ do not differ much between the bodies, we can write the ratio of the critical heat fluxes as follows

$$\frac{F_c'}{F_c} \approx \left(\frac{\sigma_y' \eta_b}{\sigma_y \eta_b'}\right)^{1/2} \quad (7)$$

where σ_y represents the yield stress and primed and unprimed variables refer to the two different bodies. For bottom-heated convection, the interior and bottom viscosities η_i and η_b are related by $\eta_i \approx 2.7\eta_b$, because the temperature drop across the bottom boundary layer is $\approx \gamma^{-1}$ (Solomatov, 1995). We therefore assume that $\eta_b/\eta_b' = \eta_i/\eta_i'$. Physically, equation (7) is reasonable: a higher yield strength requires a higher heat flux (greater convective vigour) in order for yielding to occur. On the other hand, a higher basal viscosity (lower basal temperature) causes yielding at a lower convective heat flux, other things being equal. Note that the influence of gravity is implicit in this equation, because the convective heat flux F_c depends on the Rayleigh number and thus on gravity.

O'Neill and Nimmo (2010) investigated convection with frictional faulting on Enceladus and showed that for mobile lid convection to occur required heat fluxes of about 100 mW m^{-2} and surface convective stresses ~0.1 MPa when $\eta_b = 10^{14}$ Pa s. This heat flux is similar to independent estimates based on flexural (Giese et al., 2008), crater relaxation (Bland et al., 2012), and plate-spreading (Barr, 2008) studies. Similarly, Hammond and Barr (2013) found surface convective stresses in the range 0.02-0.05 MPa and a critical heat flux of about 120 mW m^{-2} for mobile lid deformation on Ganymede taking $\eta_{\mathrm{b}} = 10^{14}$ Pa s. This result is broadly consistent with observational constraints of paleo-heat fluxes on Ganymede, which are 50 mW m^{-2} or greater (Nimmo et al., 2002; Nimmo and Pappalardo, 2004; Bland and Showman, 2007). Showman and Han (2005) showed that mobile lid convection on Europa required yield stresses in the range 0.02-0.1 MPa for a basal viscosity of 10^{13} Pa s.

Using the results summarized above, equation (7) can be used to determine the critical heat flux F_c at Pluto or Triton based on the assumed basal viscosity. However, to do so requires some understanding of whether the yield stress σ_y depends on gravity. If the effective yield stress is determined by friction on faults, larger bodies with bigger g might have higher yield stresses (Van Heck and Tackley, 2011) and require higher heat fluxes for yielding to occur (equation 7). However, the fact that the observational constraints for heat flux on Ganymede are (if anything) smaller than inferred heat fluxes on Enceladus suggests that the effective yield stress is not gravity-dependent. We will therefore assume that $\sigma'_y \approx \sigma_y$ in equation (7), and based on the Enceladus example take $\eta'_b = 10^{14}$ Pa s and $F'_c = 100$ mW m^{-2}. If we had instead based our results on the Ganymede numbers from Hammond and Barr (2013), the required heat fluxes to cause yielding would have been a factor of roughly two larger.

Equation (7) shows that for yielding to occur a relatively high interior viscosity is desirable - but too high a viscosity will shut down convection entirely. This tradeoff is illustrated in Fig 2, where the minimum shell thickness required for convection to occur (equations 4 and 5) and the critical heat flux for yielding to occur (equation 7) are plotted for various basal temperatures T_b. Here we are assuming that heat production and (convective) heat transfer are in balance. As T_b increases, η_b decreases and so the shell thickness required for convection to occur decreases. On the other hand, higher basal temperatures require higher heat fluxes to generate stresses large enough to cause yielding (equation 7). As a result, there is a restricted region in parameter space in which convection-driven yielding can occur for likely shell thicknesses. Yielding requires moderate to high heat fluxes, with higher fluxes being required at higher values of T_b.

Fig 2a shows that if the heat flux is due only to stored radiogenic heat (≈ 4 mW m^{-2}; see Fig 1), yielding is not going to occur given the shell thickness of Triton. On the other hand, if convection is transporting 18 mW m^{-2}, a basal temperature $T_b \approx 240$ K and $d \approx$300 km will allow convection and yielding to occur. At $T_b > 245$ K, convection can occur but the viscosities are too low to cause yielding. Similar results apply if the reference viscosity is 10^{15} Pa s (Fig 2b), except that everything is shifted to higher basal temperatures.

An important consequence of these results is that for yielding to occur, Triton's putative ocean must be relatively cold, presumably due to the presence of antifreeze. Ammonia is one such substance: an ocean temperature of 240-250 K at 200 MPa implies that the ocean contains 2-10 wt% NH_3 (Hogenboom et al., 1997). These kinds of ammonia concentrations are in line with theoretical predictions based on cosmochemical abundances (Lunine and Stevenson, 1987; Desch et al., 2009), especially if the ammonia has become concentrated in the ocean as the ice shell thickened.

As we discuss next, there are reasons to expect tidal dissipation in Triton to be able to generate up to ≈ 15 mW m^{-2} of heating. For a shell thickness of 300 km, surface yielding and mobile lid convection can be driven by this rate of heat transfer. Conversely, radiogenic heating alone is not capable of causing yielding.

We can provide a crude reality check on this calculation by considering Ganymede and Callisto. Both bodies had surface radiogenic heat fluxes of about $15 - 20$ mW m^{-2} four billion years ago (Schubert et al., 2004; McKinnon, 2006), comparable to our estimate for Triton at the present day. Stagnant lid convection with a low basal viscosity and mobile lid convection with a higher viscosity can yield equal heat fluxes (Solomatov, 1995). Callisto, with a basal viscosity of 10^{14} Pa s, would permit heat fluxes of about 15 mW m^{-2} via stagnant lid convection (McKinnon, 2006). However, the stresses would be too low to permit yielding and surface deformation. By our hypothesis Triton has a higher basal viscosity, which permits yielding and mobile lid convection to occur, and results in a similar rate of heat transfer. A key difference between Callisto and Triton is thus the ocean temperature, which is mainly a function of the amount of ammonia present. We infer colder ocean temperatures at Triton than Callisto, in line with the expectation that the Jovian environment was less NH_3-rich than more distant regions (Prinn and Fegley, 1981, e.g.). At Ganymede, Fig 2 shows that the inferred ancient heat flux of ~ 100 mW m^{-2} would permit both convection and yielding to occur for a warm ($\approx$270 K) ocean even in the case of a relatively thin (100 km) shell. We thus regard our arguments as plausible, but acknowledge the desirability of future numerical models to further test the likelihood of mobile lid convection under Triton conditions

3.3 Present-day tidal heating

The most important aspect of Triton's inclined orbit is that as a consequence its obliquity (angle between the rotation pole and the orbit normal) is expected to be a few tenths of a degree. A finite obliquity is important because it provides an additional source of tidal heating (Jankowski et al., 1989) in addition to the well known eccentricity tides. This is explained in more detail below.

3.3.1 Triton's obliquity

For a moderately dissipative synchronous satellite on an inclined orbit, the obliquity is driven towards an equilibrium value at which the satellite spin axis and orbit normal remain coplanar with respect to the invariable plane as they precess - a so-called Cassini state (Jankowski et al., 1989, e.g.). The orbit precession period (of 690 years) is well known (Jacobson, 2009). However, to predict the obliquity, the difference between the polar and equatorial moments of inertia of the satellite is required (because it affects the spin pole precession rate), and this moment difference is usually unknown. The usual solution is to invoke the hydrostatic assumption, which means that the body has relaxed to its long-term (strengthless) state. In this case, given an assumed polar moment of inertia, the moment of inertia difference and hence the obliquity may be derived by use of the Radau-Darwin equation (Murray and Dermott, 1999).

Triton began life hot (see above) and is not much smaller than Europa, which is demonstrably hydrostatic (Schubert et al., 2004). The available shape data for Triton, while uncertain, are consistent with a hydrostatic body (Thomas, 2000). The hydrostatic assumption for Triton is therefore not unreasonable.

Taking a dimensionless moment of inertia of 0.33, Chen et al. (2014) predicted an obliquity of 0.35° for a solid Triton; Chyba et al. (1989) obtained a similar value of 0.26° using pre-Voyager data. Chen et al. (2014) also pointed out that this value was likely to be an underestimate if Triton possessed an ocean, because in that case the shell is decoupled from the interior and the obliquity is increased. One possible example of this effect is Titan, where the measured obliquity is more than twice the predicted value based on a solid-body assumption (Bills and Nimmo, 2011). The obliquity of Triton with a decoupled shell would be approximately 0.7° (Chen et al., 2014). This factor of two difference is important because tidal heating goes as the cube of obliquity (see below).

3.3.2 Solid Body Tidal Heating

The rate of tidal dissipation in a solid, synchronous satellite is given by (Chyba et al., 1989, e.g.)

$$\dot{E}_{solid} = \frac{3}{2}\frac{k_2}{Q}\frac{n^5 R^5}{G}\left(7e^2 + \theta^2\right). \tag{8}$$

Here θ and e are the obliquity and eccentricity (both assumed small), k_2 is the degree-2 tidal Love number, Q is the dissipation factor, n is the mean motion, R is the satellite radius and G the gravitational constant. Because Triton's eccentricity $e \sim 10^{-5}$, equation (8) shows that even for $\theta = 0.1°$, obliquity tidal heating will dominate by a factor of $\sim 10^4$.

Equation (8) can be used to determine the ratio of the eccentricity damping timescale τ_e to the inclination damping timescale τ_i, assuming dissipation in the satellite dominates. The result is (Murray and Dermott, 1999)

$$\frac{\tau_i}{\tau_e} = 7\left(\frac{\sin i}{\sin\theta}\right)^2\left(\frac{1}{\cos i}\right)\frac{1}{f} \tag{9}$$

where i is the inclination and the final parameter f (≥ 1) takes into account the fact that the total obliquity tidal heating may exceed the solid body obliquity heating if an ocean is present (see below). Equation (9) shows that if f=1, inclination damping is always slower by a factor of at least 7 than eccentricity damping. In the cases we consider below, inclination damping is actually slower than this because $(\sin i/\sin\theta)^2 > f$.

The eccentricity damping timescale τ_e is given by Murray and Dermott (1999):

$$\tau_e = \frac{2}{21}\frac{Ga^2m}{n^3R^5(k_2/Q)} \tag{10}$$

where m is the mass of the satellite. Taking the nominal parameters given in Tables 1 and 2, we find τ_e ≈60 Myr, consistent with the rapid eccentricity damping found in the more sophisticated models of Ross and Schubert (1990).

Anticipating the results from the next sections, we find that $f \approx 180$ for $\theta = 0.7°$. This in turn gives $(\sin i/\sin\theta)^2/f \approx 6$, so that using equation (9) we obtain $\tau_i \approx 40\tau_e$, or about 2.5 Gyr. It is thus not unreasonable that Triton's eccentricity has damped, while its inclination (and obliquity) have persisted.

As noted by Chyba et al. (1989), dissipation in the primary has the opposite effect on inclination to dissipation in the satellite. Thus, primary dissipation can slow, or even reverse, the damping of inclination. For the nominal paramters given in Tables 1 and 2 and $\theta = 0.7°$, dissipation in the satellite dominates by a factor of 3, where we take the k_2 of Neptune to be 0.2 (Kramm et al., 2011) and use the upper bound for Q of Neptune of 36,000 (Zhang and Hamilton, 2008). If dissipation in the primary is important, our conclusion that high inclinations can have persisted is reinforced.

3.3.3 Ocean Tidal Heating

Satellites which possess oceans may undergo turbulent tidal dissipation within those oceans. Obliquity-driven tides propagating in the opposite direction to the satellite's spin are especially likely to result in dissipation, because they have a resonant frequency equal to the orbital frequency of the satellite (Tyler, 2008). In Chen et al. (2014) we have modified the formulation used in Tyler (2011) to derive ocean dissipation rates as a function of the dimensionless bottom drag parameter C_D. The drag coefficient formulation has a long history in terrestrial oceanic studies (Taylor, 1920; Jayne and Laurent, 2001, e.g.) and is relatively well-constrained ($C_D \approx 0.002$). Although it is expected to vary slightly with Reynolds number, Sohl et al. (1995) concluded that values of C_D in the range 0.002-0.01 are likely appropriate for Titan's ocean. We will adopt C_D=0.002 to be conservative here. Below we will focus on obliquity heating, since eccentricity heating in oceans is always small (Chen et al., 2014). We assume that the thickness of the ocean is large compared to the bottom topography.

One potential complication that we ignore is the role of the ice shell. A thick, rigid lid will reduce the amplitude of the obliquity tide, and hence the amount of tidal heating (Matsuyama, 2012). A Triton based on Table 1 consisting of a rigid rock-iron core overlain by a strengthless H_2O layer would have a Love number k_2=0.39. If the H_2O layer instead consisted of a 20 km thick ocean overlain by a 327 km thick convecting layer (viscosity 10^{14} Pa s, rigidity 3 GPa), k_2 is reduced to 0.20. Because converting from k_2 to ocean dissipation is not straightforward, we ignore this potential effect below, but note that it may be important to include in future.

After a certain amount of algebra, the oceanic dissipation rate $\dot{E}_{ocean}$ due to obliquity tides for Triton can be expressed as

$$\dot{E}_{ocean} \approx 8\pi\rho_w R^5 C_D n^3 \theta^3 \approx 100\ GW \left(\frac{C_D}{0.002}\right)\left(\frac{\theta}{0.35^\circ}\right)^3 \tag{11}$$

where ρ_w is the fluid density. Here we have simplified the full solutions of Chen et al. (2014) by assuming that on Triton the quantity $C_D g\theta/n^2 R \ll 1$, which is only approximately correct. Comparison with the full solutions (see below) show that the result is a slight over-estimation of the heating rate. We nonetheless show equation (11) because it makes the underlying physics more transparent. For instance, the dependence on obliquity θ is cubic, so that an uncertainty of a factor of 2 in the obliquity can make a big difference.

Making use of equations (8) and (11) we may derive the ratio of obliquity tidal heating in the solid to that in the ocean:

$$\frac{E_{ocean}}{E_{solid}} = 4\frac{\rho_w}{\bar{\rho}_p}\left(\frac{a}{R_p}\right)^3 \frac{C_D\theta}{k_2/Q} = 90\left(\frac{\theta}{0.35^\circ}\right)\left(\frac{10^{-3}}{k_2/Q}\right) = f - 1 \tag{12}$$

where here $\bar{\rho}_p$ and R_p are the bulk density and radius of the primary (Neptune) and a is the semi-major axis. Equation (12) makes physical sense: for instance, ocean dissipation is more important if the drag coefficient or the fluid density are large. It also shows that we are most likely justified in neglecting solid body dissipation compared to ocean dissipation (since $f > 1$).

Fig 3 plots ocean tidal heating as a function of obliquity θ both for the approximate expression (equation 11) and for the full solution. As noted above, the approximate expression somewhat overestimates the true dissipation rate. Nonetheless, it does accurately capture the strong (roughly cubic) dependence of dissipation on obliquity. For the nominal solid-body obliquity (0.35°), Fig 3 shows that the ocean tidal heating is comparable to the likely present-day rate of radiogenic heating (Fig 1). However, as discussed above, a more likely obliquity for a decoupled, ocean-bearing Triton is 0.7°, in which case the ocean heating rate is 320 GW (14 mW m^{-2}) assuming $C_D = 0.002$. Thus, depending on the obliquity, the likely surface heat flux from the combination of stored radiogenic heat and ocean tidal heating is 7-18 mW m^{-2}, with the higher value being more probable. As discussed in Section 3.2 above, the higher values are sufficient to cause convection and surface yielding (Fig 2), compatible with the observational constraints. Similar heat fluxes at ancient Callisto - assuming an ocean temperature ≈270 K - could have been associated with convection, but not yielding.

Because we are assuming that for Triton the convective heat flux balances the total (tidal + radiogenic) heat production, this is a steady-state situation: as long as the tidal heating is available, a long-lived ocean is compatible with mobile-lid convection. The situation is also potentially self-regulating. If too much heat is being extracted across the shell compared to the heat input from below, shell solidification will concentrate NH_3 in the remaining ocean, reducing its temperature. As a result, convection will decline in vigour, and the ocean will heat back up. This self-regulation may explain how the relatively narrow temperature range consistent with convective yielding ($T_b \approx 240$ K for the nominal parameters) could have been maintained at Triton. More sophisticated coupled thermal-orbital models would be required to address this issue further.

4 Implications for Pluto

Figure 2 summarizes the key results of this MS: for Triton, radiogenic heating alone is incompatible with convection-driven surface yielding. Conversely, with the addition of obliquity tidal heating in a subsurface ocean, convection-driven yielding is likely to occur if the ocean contains suitable concentrations of antifreeze and the ice shell is sufficiently thick. Triton likely possesses a convecting ice shell above a long-lived, cold, dissipative ocean, with the long-term evolution of the system being determined primarily by the slow damping of the orbital inclination (equation 9).

How does this scenario inform our understanding of Pluto? In our view, the key difference to Pluto is *not* that Triton started life hot (Section 3.1), but rather that its present-day orbital configuration is so different (Section 3.3). In particular, tides raised by Neptune on Triton are important, while tides raised by Charon on Pluto are expected to have almost no effect. The size of the static tidal bulge depends on the quantity $(m_p/m)(R/a)^3$ and is an order of magnitude larger for Triton than for Pluto. Furthermore, Triton's highly inclined orbit results in a relatively large predicted obliquity, while Pluto's obliquity - although unknown - is expected to be much smaller. Thus, we expect obliquity-driven tidal heating to be overwhelmingly more important on Triton than on Pluto (or almost anywhere else). In this view, Triton's unusually active present is a consequence of its unusual orbital configuration (high inclination).

If Pluto's ice shell is conductive, it may well be covering an ocean (Robuchon and Nimmo, 2011). However, radiogenic heating in Pluto's interior is insufficient to allow yielding of the ice shell, even assuming that convection is taking place (Fig 2). As a result, the young surface age and tectonic deformation seen on Triton are not predicted for Pluto. This is not to say that Pluto will have no tectonic features: ocean freezing and thermal expansion/contraction can both generate large stresses resulting in tectonics (Robuchon and Nimmo, 2011) and potentially even cryovolcanism (Manga and Wang, 2007). But such tectonic activity is likely to be ancient, so we do not expect to see the lightly-cratered, heavily resurfaced terrains characteristic of Triton. We also note that Triton's geyser activity is plausibly driven by sunlight (Kirk et al., 1990), so that analogous plumes are possible on Pluto even in the absence of ongoing endogenic activity.

5 Discussion

We have argued above that Triton is unusually active because of heating caused by its unusual orbit around Neptune; the corollary is that Pluto will not be active.

One potential flaw in this logic is that Triton might have been captured recently; for instance, Fig 1b shows that a heat flux > 10 mW m^{-2} could be sustained for 1 Gyr. Recent capture could thus explain ongoing activity, but (as noted in Section 1.2) this is considered a low-probability event. Another possibility is that Triton's young surface age might be due primarily to cryovolcanism, rather than convective yielding as we have assumed. This would certainly change the details of the argument. However, even in this case the overall logic that higher heating leads to more resurfacing is probably robust, making it likely that Pluto's surface will be much older and less active than Triton's.

More interesting is to consider the possibility that Pluto ultimately confounds our expectations and shows evidence for recent tectonic activity. We can think of at least three possible explanations for this eventuality.

Perhaps the likeliest possibility is that the potentially volatile-rich nature of Pluto's interior could affect its ability to deform. On Earth, the presence of fluids lubricates faults, reducing the effective yield stress of the near-surface material and permitting surface deformation. Analogously, antifreezes such as NH_3 (which we argue is present within Triton's ocean - Section 3.2) could permit fluid pockets to persist to relatively shallow depths within Pluto's shell, thereby weakening it (Arakawa and Maeno, 1994). Alternatively, CO_2 ice is significantly less resistive to flow than water ice under the same conditions (Durham et al., 1999), and could make it easier for surface deformation to occur. As noted in Section 1, Triton's early intense heating may have removed some of these volatile ices, but Pluto should still possess its full complement of volatiles.

A second intriguing possibility is that Pluto has not fully differentiated. Pluto's energy of accretion is not sufficient to guarantee differentiation, and nor is the putative Charon-forming impact (Canup, 2005). As pointed out by Rubin et al. (2013), a near-surface rock-rich layer would become unstable on a timescale controlled by the viscosity of the material beneath. Something similar may have happened at Triton to create the cantaloupe terrain (Schenk and Jackson, 1993). In theory, this kind of process could be responsible for recent activity at Pluto, although it would require fine-tuning (and an explanation for how it also happened recently at Triton).

A final possibility is that Pluto does in fact experience tidal heating. For instance, if its obliquity relative to Charon's orbit is sufficiently large, tidal heating could result. Of course, the fact that Charon is so small limits the effectiveness of such heating, while dissipation is hard to sustain absent some kind of resonant forcing (Murray and Dermott, 1999). Furthermore, the apparently low mutual inclinations of Pluto and Charon make this possibility unlikely, but we include it for completeness.

In conclusion, we view Triton's unusual activity as stemming from its unusual orbit. We thus anticipate that Pluto will not resemble Triton; it is more likely to resemble bodies like Rhea which do not appear to have undergone significant tidal deformation but have nonetheless experienced some ancient deformation. We would, however, be delighted to be proved wrong, and await the results from *New Horizons* with great anticipation.

Acknowledgments

We thank an anonymous reviewer and especially Sasawata Hier-Majumder for helpful comments and discussion.

References

Agnor, C. B., Hamilton, D. P., 2006. Neptune's capture of its moon Triton in a binary-planetary gravitational encounter. Nature 441, 192–194.

Arakawa, M., Maeno, N., 1994. Effective viscosity of partially melted ice in the ammonia-water system. Geophys. Res. Lett. 21, 1515–1518.

Barr, A., 2008. Mobile lid convection beneath Enceladus' south polar terrain. J. Geophys. Res. 113, E07009.

Barr, A., McKinnon, W. B., 2007. Convection in ice I shells and mantles with self-consistent grain size. J. Geophys. Res. 112, E02012.

Bills, B. G., Nimmo, F., 2011. Rotational dynamics and internal structure of Titan. Icarus 214, 351–355.

Bland, M. T., Showman, A. P., 2007. The formation of Ganymede's grooved terrain: Numerical modeling of extensional necking instabilities. Icarus 189, 439–456.

Bland, M. T., Singer, K. N., McKinnon, W. B., Schenk, P. M., 2012. Enceladus' extreme heat flux as revealed by its relaxed craters. Geophys. Res. Lett. 39, L17204.

Brown, R. H., Johnson, T. V., Goguen, J. D., Schubert, G., Ross, M. N., 1991. Triton's global heat budget. Science 251, 1465–1467.

Buie, M. W., Tholen, D. J., Grundy, W. M., 2012. The orbit of Charon is circular. Astron. J. 144, 15.

Canup, R. M., 2005. A giant impact origin of Pluto-Charon. Science 307, 546–550.

Carslaw, H. S., Jaeger, J. C., 1986. Conduction of heat in solids. Oxford University Press.

Chen, E. M. A., Nimmo, F., Glatzmaier, G. A., 2014. Tidal heating in icy satellite oceans. Icarus 229, 11–40.

Chyba, C. F., Jankowski, D. G., Nicholson, P. D., 1989. Tidal evolution in the Neptune-Triton system. Astron. Astrophys. 219, L23–L26.

Croft, S. K., Kargel, J. S., Kirk, R. L., Moore, J. M., Schenk, P. M., Strom, R. G., 1995. The geology of Triton. In: Cruikshank, D. P. (Ed.), Neptune and Triton. Univ. Arizona Press, pp. 879–947.

Cuk, M., Gladman, B. J., 2005. Constraints on the orbital evolution of Triton. Astrophys. J. 626, L113–L116.

Desch, S. J., Cook, J. C., Doggett, T., Porter, S. B., 2009. Thermal evolution of Kuiper Belt Objects with implications for cryovolcanism. Icarus 202, 694–714.

Durham, W. B., Kirby, S. H., Stern, L. A., 1999. Steady-state flow of solid CO2: Preliminary results. Geophys. Res. Lett. 26, 3493–3496.

Durham, W. B., Prieto-Ballesteros, O., Goldsby, D. L., Kargel, J. S., 2010. Rheological and thermal properties of icy materials. Space Sci. Rev. 153, 273–298.

Gaeman, J., Hier-Majumder, S., Roberts, J. H., 2012. Sustainability of a subsurface ocean within Triton's interior. Icarus 220, 339–347.

Giese, B., Wagner, R., Hussmann, H., Neukum, G., Perry, J., Helfenstein, P., Thomas, P. C., 2008. Enceladus: An estimate of heat flux and lithospheric thickness from flexurally supported topography. Geophys. Res. Lett. 35, L24204.

Goldreich, P., Murray, N., Longaretti, P. Y., Banfield, D., 1989. Neptune's story. Science 245, 500–504.

Goldsby, D. L., Kohlstedt, D. L., 2001. Superplastic deformation of ice: Experimental observations. J. Geophys. Res. 106, 11017–11030.

Hammond, N. P., Barr, A. C., 2013. Formation of Ganymede's grooved terrain by convection-driven resurfacing. Icarus .

Hogenboom, D. L., Kargel, J. S., Consolmagno, G. J., Holden, T. C., Lee, L., Buyyounouski, M., 1997. The ammonia-water system and the chemical differentiation of icy satellites. Icarus 128, 171–180.

Hussmann, H., Sohl, F., Spohn, T., 2006. Subsurface oceans and deep interiors of medium-sized outer planet satellites and large trans-neptunian objects. Icarus 185, 258–273.

Jacobson, R. A., 2009. The orbits of the Neptunian satellites and the orientation of the pole of Neptune. Astron. J. 137, 4322–4329.

Jankowski, D. G., Chyba, C. F., Nicholson, P. D., 1989. On the obliquity and tidal heating of Triton. Icarus 80, 211–219.

Jayne, S. R., Laurent, L. C. S., 2001. Paramterizing tidal dissipation over rough topography. Geophys. Res. Lett. 28, 211–219.

Kirk, R. L., Brown, R. H., Soderblom, L. A., 1990. Subsurface energy storage and transport for solar-powered geysers on Triton. Science 250, 424–429.

Klinger, J., 1980. Influence of a phase transition of ice on the heat and mass balance of comets. Science 209, 271–272.

Kramm, U., Nettelmann, N., Redmer, R., Stevenson, D. J., 2011. On the degeneracy of the tidal Love number k2 in multi-layer planetary models: application to Saturn and GJ436b. Astron. Astrophys. 528, A18.

Lunine, J. I., Stevenson, D. J., 1987. Clathrate and ammonia hydrates at high pressure: Application to the origin of methane on Titan. Icarus 70, 61–77.

Manga, M., Wang, C.-Y., 2007. Pressurized oceans and the eruption of liquid water on Europa and Enceladus. Geophys. Res. Lett. 34, L07202.

Matsuyama, I., 2012. Tidal dissipation in the subsurface oceans of icy satellites. Lunar Planet. Sci. Conf. 43, 2068.

McKinnon, W., Leith, A. C., 1995. Gas drag and the orbital evolution of a captured Triton. Icarus 118, 392–413.

McKinnon, W. B., 2006. On convection in ice I shells of outer solar system bodies, with detailed application to Callisto. Icarus 183, 435–450.

McKinnon, W. B., Kirk, R. L., 2007. Triton. In: McFadden, L.-A., Weissman, P. R., Johnson, T. V. (Eds.), Encyclopedia of the solar system. Academic Press, pp. 483–502.

Moresi, L., Solomatov, V., 1998. Mantle convection with a brittle lithosphere: thoughts on the global tectonic styles of Earth and Venus. Geophys. J. Int. 133, 669–682.

Murray, C. D., Dermott, S. F., 1999. Solar System Dynamics. Cambridge Univ. Press.

Nimmo, F., Pappalardo, R. T., 2004. Furrow flexure and ancient heat flux on Ganymede. Geophys. Res. Lett. 31, L19701.

Nimmo, F., Pappalardo, R. T., Giese, B., 2002. Effective elastic thickness and heat flux estimates on Ganymede. Geophys. Res. Lett. 29, 1158.

O'Neill, C., Nimmo, F., 2010. The role of episodic overturn in generating the surface geology and heat flow on Enceladus. Nature Geosci. 3, 88–91.

Porco, C. C., et al., 2006. Cassini observes the active south pole of Enceladus. Science 311, 1393–1401.

Prinn, R. G., Fegley, B., 1981. Kinetic inhibition of CO and N2 reduction in circumplanetary nebulae - implications for satellite composition. Astrophys. J. 24, 308–317.

Robuchon, G., Nimmo, F., 2011. Thermal evolution of Pluto and implications for surface teconics and a subsurface ocean. Icarus 216, 426–439.

Ross, M. N., Schubert, G., 1990. The coupled orbital and thermal evolution of Triton. Geophys. Res. Lett. 17, 1749–1752.

Rubin, M. E., Desch, S. J., Neveu, M., 2013. Limits on the overturn of undifferentiated crust on Kuiper Belt Objects due to Rayligh-Taylor instabilities. Icarus submitted.

Schenk, P. M., Jackson, M. P. A., 1993. Diapirism on Triton: a record of crustal layering and instability. Geology 21, 299–302.

Schenk, P. M., Zahnle, K., 2007. On the negligible surface age of Triton. Icarus 192, 135–149.

Schubert, G., Anderson, J. D., Spohn, T., McKinnon, W. B., 2004. Interior composition, structure and dynamics of the Galilean satellites. In: Bagenal, F., Dowling, T., McKinnon, W. (Eds.), Jupiter: The planet, satellites and magnetosphere. Cambridge Univ. Press, pp. 281–306.

Showman, A. P., Han, L., 2005. Effects of plasticity on convection in an ice shell: Implications for Europa. Icarus 177, 425–437.

Sohl, F., Sears, W. D., Lorenz, R. D., 1995. Tidal dissipation on Titan. Icarus 115, 278–294.

Solomatov, V. S., 1995. Scaling of temperature-dependent and stress-dependent viscosity convection.

Phys. Fluids 7, 266–274.
Stern, S. A., McKinnon, W. B., 2000. Triton's surface age and impactor population revised in light of Kuiper belt fluxes: Evidence for small Kuiper belt objects and recent geological activity. Astron. J. 119, 945–952.
Taylor, G. I., 1920. Tidal friction in the Irish Sea. Phil. Trans. R. Soc. A 220, 1–33.
Thomas, P. C., 2000. The shape of Triton from limb profiles. Icarus 148, 587–588.
Turcotte, D. L., Schubert, G., 2002. Geodynamics, 2nd Edition. Cambridge University Press.
Tyler, R., 2011. Tidal dynamical considerations constrain the state of an ocean on Enceladus. Icarus 211, 770–779.
Tyler, R. H., 2008. Strong ocean tidal flow and heating on moons of the outer planets. Nature 456, 770–772.
Van Heck, H. J., Tackley, P. J., 2011. Plate tectonics on super-Earths: Equally or more likely than on Earth. Earth Planet. Sci. Lett. 310, 252–261.
Vokrouhlicky, D., Nesvorny, D., Levison, H. F., 2008. Irregular satellite capture by exchange reactions. Astron. J. 136, 1463–1476.
Zahnle, K., Schenk, P., Levison, H., Dones, L., 2003. Cratering rates in the outer solar system. Icarus 163, 263–289.
Zhang, K., Hamilton, D. P., 2008. Orbital resonances in the inner neptunian system II: Resonant history of Proteus, Larissa, Galatea and Despina. Icarus 193, 267–282.

A Appendix: Description of numerical code

Here we outline our model of the thermal evolution of a multi-layered, conductive body used to produce the results shown in Fig 1. Our approach resembles that of Robuchon and Nimmo (2011), except that we do not consider convection and can thus adopt a 1-D approach. The heat conduction equation in spherical coordinates is

$$\frac{\partial T}{\partial t} = \frac{\kappa}{r^2}\frac{\partial}{\partial r}\left(r^2\frac{\partial T}{\partial r}\right) + \frac{H}{C_p} \tag{1}$$

where κ is the thermal diffusivity (assumed constant), H is the heat production rate in W kg^{-1} and C_p is the specific heat capacity. The heat production rate in the rock-iron core is calculated as in Robuchon and Nimmo (2011).

In the rock-iron core we solve equation (1) using a finite-difference scheme on 100 nodes with a constant node spacing Δr_c. The inner boundary condition is zero temperature gradient. The outer boundary condition depends on whether an ocean is present. In the absence of an ocean, the top node of the core is also the bottom node of the ice shell. If an ocean is present, the top node of the core has a temperature set to the ocean temperature (273 K). The specific heat capacity of the core is 1053 J kg^{-1} K^{-1} and $\kappa_c = 1.1 \times 10^{-6}$ m^2 s^{-1}.

Initially, the entire ice shell will be frozen. In this case, we use equation (1) in the shell, taking into account the radial step-change in thermal properties at the ice-core interface and setting the heat production term to zero in the shell (Gaeman et al., 2012, cf.). We use 100 nodes with fixed spacing Δr; ice shell parameters are given in Table 2. The timestep Δt used in our numerical model is the smaller of $0.03\Delta r^2/\kappa$ and $0.03\Delta r_c^2/\kappa_c$.

When modelling the effects of melting and freezing, to avoid numerical instabilities we assume that both occur linearly across a temperature range from $T_m - \Delta T_m$ to T_m, where T_m=273 K and

ΔT_m=3 K. The energy density required for complete melting is given by $E_0 = \rho_i(C_p\Delta T_m + L_H)$, where L_H is the latent heat of fusion (0.33 MJ/kg) and $C_p = 1970$ J kg^{-1} K^{-1}.

Melting is assumed to start at the lowermost ice node and to go to completion within each node before melting begins in the next node above. Each node has an initial energy content $E^i = 0$. For the melting node, for each timestep at which the predicted temperature in the node T^i equals or exceeds $T_m - \Delta T_m$, we increment E^i by an amount ΔE^i where

$$\Delta E^i = \frac{\Delta t}{\Delta r}\left(F_b^i - \frac{k(T^i - T^{i+1})}{\Delta r}\right) \tag{2}$$

If the node below is rock-iron, then the basal heatflux F_b^i can be calculated using the usual conduction approach and equation (2) resembles a finite-difference version of equation (1). If an ocean is present, we assume that heat transfer across the ocean is instantaneous, in which case we have

$$F_b^i = \left(\frac{R_s}{r^i}\right)^2 F_c \tag{3}$$

where r^i is the radial position of the i-th (melting) node, R_s is the radius of the rock-iron core and F_c is the conductive heat flux out of the core.

When a particular node is melting, the melt fraction $\phi^i = E^i/E_0$ and the temperature is $T^i = T_m - (1-\phi^i)\Delta T_m$. If melting goes to completion, that node is then assigned to be part of the ocean (temperature T_m) and is no longer treated with equation (2); melting begins at the next node above. Because melting is discretized (only one node melts at a time), the heat flux across the base of the shell is also discretized, resulting in the stair-step pattern seen in Fig 1.

Freezing is modelled in an analogous fashion. If the change in energy given by equation (2) is negative, freezing is occurring and the melt fraction ϕ^i and temperature T^i are both reduced. When $E^i = 0$, freezing has gone to completion on the i-th node, and equation (2) is then applied to the next node down.

To ensure that our code was working correctly, we compared our results with the conductive case shown in Fig 2 of Robuchon and Nimmo (2011). The agreement was excellent, except for a brief period after the episode of tidal heating included in the calculations of Robuchon and Nimmo (2011), but neglected in our model. We also checked our solution against the analytical (Cartesian) Stefan solution (Turcotte and Schubert, 2002) by setting the heat flux out of the core to zero after 30 Myr (to allow initial melting) and allowing the shell to evolve conductively. Using the thermal parameter values of Gaeman et al. (2012) for which the quantity $\lambda = 0.72$ we found a shell thickness of 247 km after 300 Myr, which is within 3% of the analytical value of 254 km.

Qty.	Triton	Pluto	Units	Eqn.	Qty.	Triton	Pluto	Units	Eqn.
R	1353	1153	km	1	ρ_b	2061	2030	kg m^{-3}	1
R_s	1026	866	km	1	d_{max}	327	287	km	-
g	0.779	0.658	m s^{-2}	4	P	5.877	6.387	days	-
e	0.000016	<0.000075[a]	-	8	i	156.87°	0[b]	-	9
T_s	38	44	K	4	a	355,000	19,573	km	2
R_p	25,300	-	km	-	m_p	1.02×10^{26}	1.52×10^{21}	kg	2

Table 1

Parameter values for Triton and Pluto. "Eqn."=equation, "Qty."=quantity. For Pluto, orbital parameters (P,e,m_p,i,a) are for the relevant tide-raising body (Charon). [a] upper limit from Buie et al. (2012). [b] Inclination of Charon relative to Pluto rotation axis. This has not been measured but is expected to be very small due to tidal damping.

Qty.	Symbol	Value	Units	Eqn.
Thermal conductivity	k	3	W m^{-1} K^{-1}	6
Thermal expansivity	α	10^{-4}	K^{-1}	4
Ice density	ρ_i	950	kg m^{-3}	1
Water density	ρ_w	1000	kg m^{-3}	11
Thermal diffusivity	κ	1.6×10^{-6}	m^2 s^{-1}	4
Activation energy	E_a	60	kJ/mol	3
Drag coefficient	C_D	0.002	-	11
-	k_2/Q	10^{-3}	-	8
Reference temperature	T_0	273	K	3
Reference viscosity	η_0	10^{14}	Pa s	3

Table 2

Nominal values for ice shell and other parameters of interest

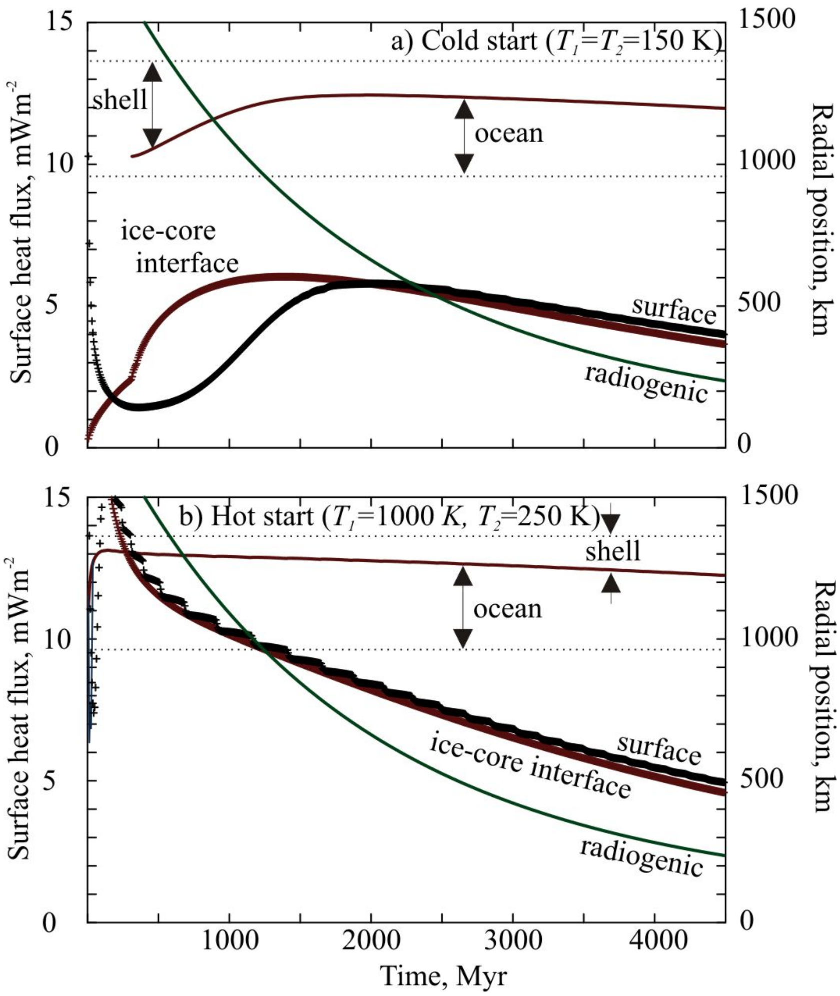

Fig. 1. Thermal evolution models for a conductive Triton showing evolution of heat fluxes and ice shell thickness (see Appendix for more details). Plotted heat fluxes are all evaluated at the surface. Shell thinning occurs when the heat flux out of the ice-core interface exceeds that across the ice shell, and vice versa. Note that the instantaneous radiogenic heat production does not equal the heat flux out of the core, because of the time it takes for heat to be conducted across the core. a) Cold start (initial temperature 150 K). b) Hot start (1000 K for core, 250 K for ice shell). Stair-step pattern in surface heat flux is due to discretization employed (see Appendix).

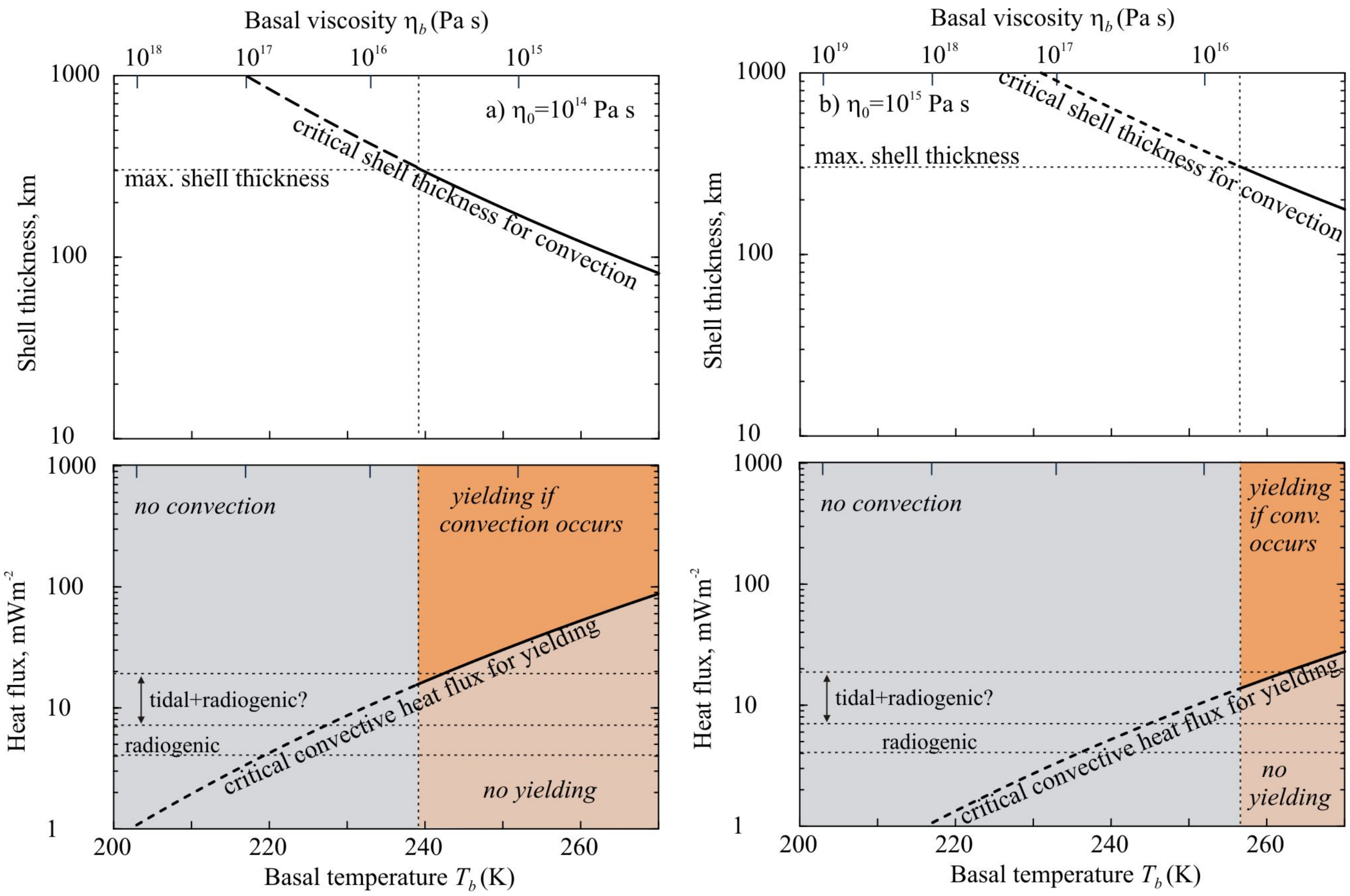

Fig. 2. Minimum shell thickness for convection to occur (equations 4 and 5) and critical heat flux for yielding to occur (equation 7) for various basal temperatures T_b. Here we assume that the basal viscosity $\eta_b = \eta_i/2.7$ (see text) and we take reference values $F_c' = 100$ mW m^{-2} and $\eta_b' = 10^{14}$ Pa s. The horizontal dashed lines in the lower panels indicate the likely radiogenic heat flux, and the likely range of heat fluxes when obliquity tidal heating is included. a) $\eta_0 = 10^{14}$ Pa s. b) $\eta_0 = 10^{15}$ Pa s

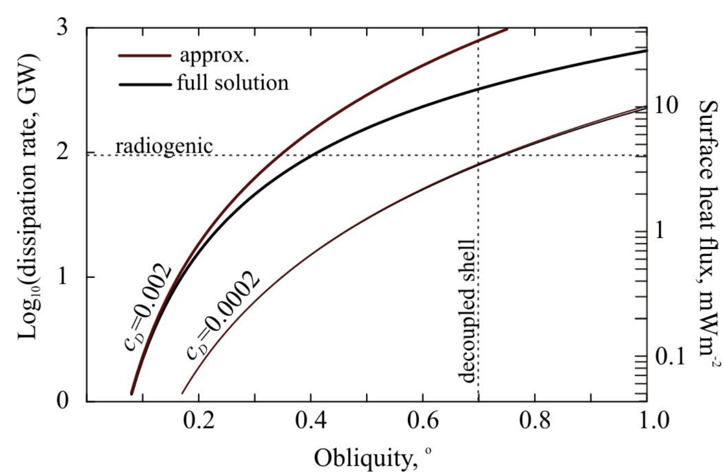

Fig. 3. Obliquity tidal heating in an ocean for different drag coefficients C_D. Red and black lines are approximation (11) and full solution (from Chen et al. (2014)), respectively.